









 Cite this: *RSC Adv.*, 2023, 13, 29363

# Facile synthesis of CuONPs using *Citrus limon* juice for enhancing antibacterial activity against methicillin-resistant *Staphylococcus aureus*, beta-lactamase and tetracycline-resistant *Escherichia coli*†

 Abdullah Rafsan,  ‡<sup>a</sup> Aminur Rahman,  ‡<sup>a</sup> Samia Akter,  <sup>a</sup> Nymul Yeachin,  <sup>b</sup> Tania Faruqe, <sup>c</sup> Gautam Kumar Deb, <sup>d</sup> Taehyeong Ha, <sup>e</sup> Khandker Saadat Hossain, <sup>b</sup> Muhammad Tofazzal Hossain,  <sup>a</sup> Md. Abdul Kafi  <sup>\*a</sup> and Jeong-Woo Choi  <sup>\*e</sup>

Antimicrobial resistance (AMR) resulting from indiscriminate use of antibiotics in various fields of agriculture such as livestock farming, aquaculture, and crop fields become an emerging catastrophe for the health (human, animal) and environment. Among those, poultry farming has been considered as one of the major contributors of multidrug-resistant (MDR) bacteria. Focusing this, the present research is designed for green synthesis of copper oxide nanoparticles (CuONPs) with the aim of their application in antibiotic-free poultry farming for curbing use of antibiotics in that sector. For that, antibacterial CuONPs were nanoformulated to decrease the required doses of bulk CuSO<sub>4</sub>. We used a CuSO<sub>4</sub>·5H<sub>2</sub>O solution as a Cu<sup>2+</sup> source and *Citrus limon* juice as a reducing agent as well as capping agent. Particle yield was initially confirmed by the λ<sub>max</sub> specific to CuONPs (295 nm) using UV-Vis spectroscopy. The presence of the Cu–O group during particle formation and crystallinity with the purity of yielded NPs was confirmed with Fourier-transform infrared spectroscopy and X-ray diffractometry. The round to spherical CuONPs of 92–155 nm average size was confirmed with atomic force, scanning electron, and transmission electron microscopy. The concentration of yielded NPs was calculated with the dynamic light scattering. The physical characterization tools indicated a maximum CuONPs yield with a 0.001 M ion source with 15% reducing agents after 12 h reduction. Antibacterial effectivity was tested against methicillin-resistant *Staphylococcus aureus* and tetracycline- and beta-lactamase-resistant *Escherichia coli*, confirmed by PCR amplicon band at 163 bp, 643 bp, and 577 bp for the *mecA*, *blaTEM-1* and *tetA* genes, respectively. An antibiogram assay of CuONPs showed a maximum zone of inhibition of 26 ± 0.5 mm for the synthesized particles. The minimum inhibitory and bactericidal concentrations were 1.6 μg ml<sup>-1</sup> and 3.1 μg ml<sup>-1</sup>, respectively, for broad-spectrum application. Finally, the biocompatibility of CuONPs was determined by demonstrating a nonsignificant decrease of BHK-21 cell viability at <2 MIC doses for complying their future *in vivo* applicability.

 Received 24th July 2023  
 Accepted 27th September 2023

DOI: 10.1039/d3ra04985j

[rsc.li/rsc-advances](http://rsc.li/rsc-advances)

## 1. Introduction

Antimicrobial resistance (AMR) represents a public health threat worldwide.<sup>1</sup> The excessive use of antibiotics in human,

veterinary medicine, and agriculture has further aggravated this situation, and an emerging public health catastrophe is being predicted.<sup>2</sup> Numerous studies have shown that the environment has already been exposed to many antimicrobial-resistant bacteria because of excess use of antibiotics in agricultural sectors including crops, livestock, and aquaculture.<sup>3,4</sup> Public health has been seriously affected by the presence of antimicrobial residues in food.<sup>5</sup> Environment exposure to such residues occurs in a wide variety of ways, such as horizontal spreading of resistant bacteria from human medical waste, livestock farms and household wastes.<sup>2</sup> This in turn results in the appearance of antimicrobial-resistant microbes, both through alteration of gene sequences as an adoptive mechanism and through transfer of resistance gene during plasmid sharing.<sup>6</sup> The antibacterial residues in various farm products

<sup>a</sup>Department of Microbiology and Hygiene, Bangladesh Agricultural University, Mymensingh-2202, Bangladesh

<sup>b</sup>Department of Physics, University of Dhaka, Dhaka-1000, Bangladesh

<sup>c</sup>Experimental Physics Division, Atomic Energy Centre, Dhaka, Bangladesh

<sup>d</sup>Department of Biotechnology, Bangladesh Livestock Research Institute, Savar, 1341, Dhaka, Bangladesh

<sup>e</sup>Department of Chemical and Biomolecular Engineering, Sogang University, Seoul 04107, Republic of Korea. E-mail: [jwchoi@sogang.ac.kr](mailto:jwchoi@sogang.ac.kr)

 † Electronic supplementary information (ESI) available. See DOI: <https://doi.org/10.1039/d3ra04985j>

‡ These authors contributed equally to the work.



that result from injudicious usage of antibiotics are therefore considered as major cause of emergence of AMR.<sup>1,6</sup> Antibiotics are usually administered as a prophylactic measure to reduce disease or bacteriological spoilage-related losses of products both on the farm and in the live animal market, without considering withdrawal periods.<sup>7</sup> Consequently, a significant amount of the applied antibiotics remains in the food chain as residue.<sup>8</sup> This situation is common in many least developed and developing countries, where agricultural farming has increased in step with socio-economic development. In addition to injudicious antibiotics use on farms, several other factors contribute to the problem including lack of public awareness regarding the use of antibiotics and lack of regulation governing antibiotic prescriptions.<sup>9</sup> AMR is thus emerging at catastrophic levels among underdeveloped nations around the world, where medically important microorganisms have frequently stopped responding to widely used antibiotic treatments.<sup>9</sup> It is therefore crucial to find appropriate measures for breaking the pattern of resistance emergence through interrupting the spread of residues and of resistant bacteria from potential farm sources.

MDR in poultry farming appears as a serious threat that resulted nonresponsive antibiotic therapy.<sup>10</sup> As a result, farmers have been using antibiotics repeatedly and indiscriminately for protecting their farms.<sup>11</sup> Such indiscriminate use of antibiotics creates several aftermath like, (i) costly production, (ii) antibiotic residue laden products, (iii) severe public health impact due to the presence antibiotic in food chain.<sup>12,13</sup> Thus, curbing use of antibiotics could be an useful step to overcome this alarming situation. A recent review enlightened about the use of antimicrobial nanomaterials for tackling such alarming situation.<sup>1</sup> Gao *et al.* 2021 suggested that with continued research and development, nanomaterials may become a mainstay for treating bacterial infections in the era of antibiotic resistance.<sup>1</sup> Hence, this research aimed on the development and applications of antimicrobial nanomaterials as an alternate of antibiotics in poultry farming. Many naturally available antimicrobial materials have already been employed for such purpose.<sup>3,14-16</sup> However, none of them found suitable because of their costly, laborious and bioincompatible extraction and nanoformulation process.<sup>17-19</sup> Therefore, a cost effective, facile, biocompatible green antibacterial nanomaterials synthesis method is critically required.

Copper sulphate ( $\text{CuSO}_4 \cdot 5\text{H}_2\text{O}$ ) is a widely used antimicrobial agent with demonstrated germicidal power.<sup>20</sup> Many studies have investigated the use of  $\text{CuSO}_4 \cdot 5\text{H}_2\text{O}$  as a feed and soil additive, sewage water treatment agent, supplementary agent for cosmetics, pesticide, fungicide, *etc.*<sup>14,21,22</sup> However, application of bulk  $\text{CuSO}_4 \cdot 5\text{H}_2\text{O}$  still faces many challenges such as high dose requirements, bio-incompatibility, corrosiveness when applied to surfaces, and high cost.<sup>23</sup> The present research focused on overcoming these limitations by enhancing functionality through nanoformulation of  $\text{CuSO}_4 \cdot 5\text{H}_2\text{O}$  and thus lower dosage requirements. Nano-formulated products (nanoparticles) offer many advantageous attributes such as increased surface areas, exposed functional groups, and enhanced ion-exchange and -absorption ability, all of which result in enhanced functionality.<sup>24-26</sup> Various studies have therefore

investigated nanoformulation of  $\text{CuSO}_4 \cdot 5\text{H}_2\text{O}$  with the aim of developing antimicrobial nanomaterials.<sup>27-30</sup> Nahar *et al.* synthesized copper(II) oxide nanoparticles (CuONPs) and evaluated their antibacterial effects against *S. aureus*.<sup>31</sup> Other researchers evaluated the antibacterial effects of CuONPs against *Klebsiella aerogenes*, *E. coli*, *S. aureus*, *Pseudomonas desmolyticum*, *Enterobacter aerogenes*, *Shigella* spp., and others.<sup>27,28,30,32,33</sup> While antibacterial activity against all these bacteria was demonstrated, the required doses still did not much differ from those of the bulk state.<sup>29</sup> The average minimum inhibitory concentration (MIC) and minimum bactericidal concentration (MBC) of previously synthesized CuONPs was 200–500  $\mu\text{g ml}^{-1}$  and 125–1000  $\mu\text{g ml}^{-1}$ , respectively, while that of the bulk state not significantly different at 200–400  $\mu\text{g ml}^{-1}$  and 400–1600  $\mu\text{g ml}^{-1}$ , respectively.<sup>31,34</sup> Current state of the art CuONPs cannot overcome the limitations of bulk  $\text{CuSO}_4 \cdot 5\text{H}_2\text{O}$  as long as they are not sustainable for low-input, maximum-output-based farming systems.<sup>22,26,35,36</sup> A nanoformulation satisfying these criteria is in urgent demand for reducing the doses of NPs used for the mitigation of the spread of environmental AMR bacteria. Moreover, while the previously synthesized NPs were able to produce an inhibitory zone against bacteria, they were not suitable for application in biological systems.<sup>36</sup> Previous synthesis protocols for CuONPs employed chemical reducing agents in their reduction process, producing cytotoxic effects, and previous research investigating the cytotoxicity of CuONPs and hybrid NPs demonstrated toxic effect against mammalian cells.<sup>21</sup> Therefore, an effective antimicrobial, biocompatible, and cost-effective nanomaterial is critically required. To this end, the present study focused on the uncomplicated synthesis of CuONPs for obtaining biocompatible antibacterial nanomaterials useable against AMR threats.

In this study, CuONPs were synthesized employing  $\text{CuSO}_4 \cdot 5\text{H}_2\text{O}$  solution as an ion source, and *Citrus limon* juice as a biocompatible reducing agent that constitutes an alternative to chemical reducing agents. The resultant nanoparticles were subjected to physical characterization through UV-Vis spectroscopic analysis, Fourier-transform infrared spectroscopy (FTIR), X-ray diffraction (XRD), atomic force microscopy (AFM), scanning electron microscopy (SEM), transmission electron microscopy (TEM), and dynamic light scattering (DLS). Then the physically confirmed nanoparticles were subjected to an evaluation of antimicrobial activity against MDR *S. aureus* and *E. coli* using antibiogram profiling after PCR detection of MDR genes. MIC and MBC of yielded NPs were determined following broth dilution methods. The biocompatibility of the yielded NPs was evaluated using BHK-21 cells following MTT assay prior to *in vivo* application for producing antibiotic-free safe poultry without incurring AMR risks.

## 2. Materials and methods

### 2.1. Materials

Copper sulphate pentahydrate ( $\text{CuSO}_4 \cdot 5\text{H}_2\text{O}$ ) was purchased from local market of Mymensingh Sadar, Bangladesh (BD). Phosphate buffered saline (PBS) and sodium chloride (NaCl) were purchased from Merck Life Science Pvt. Ltd, Mumbai,

India. Alcohol and other chemical disinfectants were purchased from the local supplier (ZH chemicals, Hatkhola, Dhaka, BD). Antibiotic disks and blotting papers were purchased from HI-Media Laboratories Pvt. Ltd, Mumbai, India. Nutrient broth, Eosin Methylene Blue agar, Mannitol Salt agar, Muller Hilton agar, Muller Hilton broth and Gram's staining materials were also purchased from Hi-Media Laboratories Pvt. Ltd, Mumbai, India. PCR master mixes were purchased from Promega, Madison, USA. Primer sets (*16s rRNA* gene, *mec* gene, *malB* gene, *blaTEM-1* gene, *tetA* gene), agarose powder, DNA ladder, Tris-Acetate-EDTA buffer, Nuclease free water, were purchased from Biotech Concern, Dhaka, BD. A total of 10 (Ten) *Staphylococcus aureus* and 10 (Ten) *Escherichia coli* stock from poultry sources were collected from the laboratory stock of the Department of Microbiology and Hygiene, BAU, and used for the present study.

## 2.2. Methods

**2.2.1. Green synthesis of copper oxide nanoparticles (CuONPs).**  $\text{CuSO}_4 \cdot 5\text{H}_2\text{O}$  solutions of various molarities (M) were prepared in deionized water (DIW) as ion source and stirred until a homogenous solution was achieved. A freshly cleaned lemon was cut and the juice was extracted using a lemon squeezer. The juice was centrifuged to remove fibres and the supernatant was collected. Various concentrations of lemon juice were added into  $\text{CuSO}_4 \cdot 5\text{H}_2\text{O}$  solution and the reduction reaction was allowed at room temperature until a visible color shift was noted. Then the solutions were centrifuged at 1300 rpm for 3 min and the supernatants were collected, then subjected to physical and biological characterization. The CuONPs formation was initiated by dissolving  $\text{CuSO}_4 \cdot 5\text{H}_2\text{O}$  in water at 100 °C and thus  $\text{Cu}^{2+}$  ions were formed (Fig. 1).<sup>37</sup> The  $\text{Cu}^{2+}$  was reduced through bonding with OH groups of  $\text{C}_6\text{H}_8\text{O}_7$  (citric acid obtained from lemon juice<sup>38</sup>) to

form  $\text{Cu}^0$ .<sup>39</sup> With the continued stirring, the  $\text{Cu}^0$  was oxidized at the presence of atmospheric oxygen to form CuO atoms.<sup>39</sup> The CuO atoms were nucleated, grown, and finally capped with the remaining citric acid to form CuONPs.<sup>40</sup>

**2.2.2. Physical characterization of CuONPs.** UV visible spectra were recorded with UV-Vis spectrophotometry (UV-1600PC, VWR, Radnor, PA, USA) at a wavelength range of 200–700 nm for the confirmation of CuONPs yield.<sup>24</sup> The UV-Vis analysis was performed every 3 h until the color of the yielded solution was fixed. Data obtained from reference solution (DIW) and synthesized CuONPs solutions were compared based on shifts of the absorption peak ( $\lambda_{\text{max}}$ ). The chemical changes and bonding between functional groups of synthesized CuONPs was confirmed with FTIR investigation (PerkinElmer, FTIR in basic mode of Golden Gate using PerkinElmer IR spectroscopy software). For X-ray diffraction (Multipurpose X-Ray Diffractometer-SmartLab) CuONPs solutions were drop casted and dried on a silicon wafer.<sup>41</sup> The samples were examined using an FTIR spectrometer (PerkinElmer, Waltham, MA, USA) recorded at resolutions from  $300 \text{ cm}^{-1}$  to  $4500 \text{ cm}^{-1}$  and scan rates of  $4\text{--}64 \text{ cm}^{-1}$  in basic mode (Golden Gate) using PerkinElmer IR spectroscopy software.<sup>42</sup> The Atomic Force Microscopy (Flex-AFM, Nanosurf, Liestal, Switzerland) was performed to determine size of the yielded particles, using non-contact mode for analyzing surface roughness. Before scanning, the CuONPs solution was spin-coated at 1300 rpm and dried at 60 °C in an oven.<sup>3</sup> The nanostructural morphology and surface topography of synthesized CuONPs was investigated using Scanning Electron Microscopy (FESEM, Hitachi S-470) and Transmission Electron Microscopy (F200X G2 TEM)<sup>43</sup> For this, a thin layer of Au was sputtered on a silicon wafer surface drop-casted with CuONPs. Images were obtained at an accelerated voltage of 10 kV and a current of 10 mA. The TEM was set with voltage of 80 kV and Ceta 16 M camera with  $4\text{k} \times 4\text{k}$  images with  $512 \times 512$  pixels at 320 fps mood.

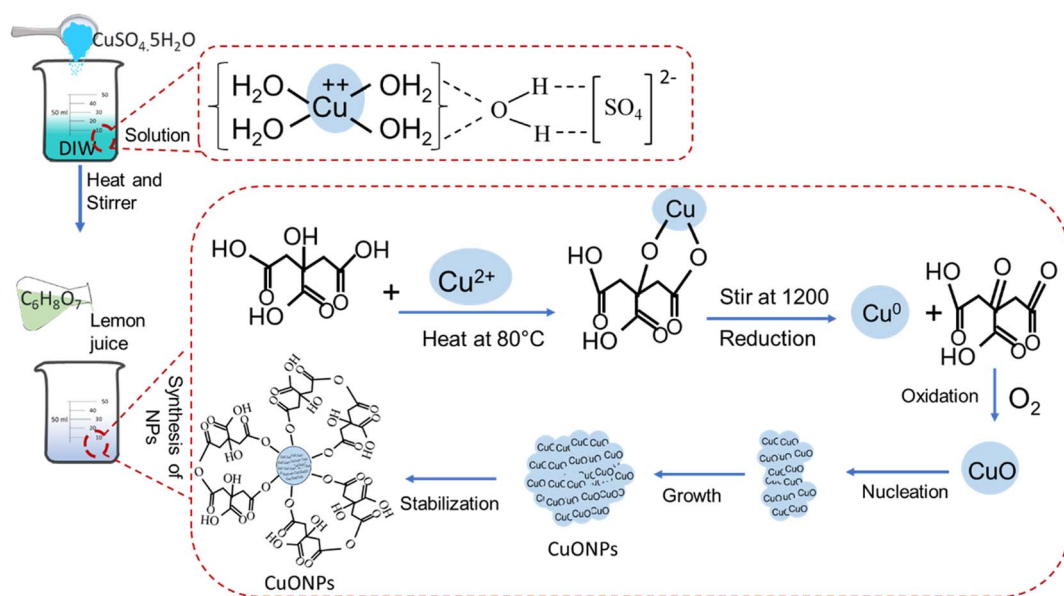


Fig. 1 Schematic illustration of CuONPs formation mechanism.

Table 1 List of primers used in this study

Target gene	Primer	Sequences (5'-3')	Amplicon size	Ref.
16srRNA	F	GTAGGTGGCAAGCGTTATCC	228 bp	46
	R	CGCACATCAGCGTCAG		
mecA	F	ACTGCTATCCACCCTCAAAC	163 bp	47
	R	CTGGTGAAGTTGTAATCTGT		
malB	F	GACCTCGGTTTAGTTCACAGA	585 bp	48
	R	CACACGCTGACGCTGACCA		
blaTEM-1	F	ACTCCCCGTCGTGTAGATAA	643 bp	49
	R	TGGCCGTTGCCGTTATCTAC		
tetA	F	GGTTCACCTCGAACGACGTCA	577 bp	50
	R	CTGTCCGACAAGTTGCATGA		

**2.2.3. Identification and characterization of revived *S. aureus* and *E. coli*.** Ten bacterial samples from laboratory stock were reconfirmed by colony morphology, staining properties, and molecular detection.<sup>44</sup> For colony characteristic of *S. aureus* and *E. coli*, isolates were streaked on mannitol salt agar (MSA) media and eosinophil methylene blue (EMB) agar media and incubated at 37 °C for 24 h. For microscopic characterization, pure single colonies were selected from MSA and EMB and stained with gram's staining materials following standard procedures.<sup>3</sup> Bacterial DNA for molecular characterization was extracted using the boiling method.<sup>45</sup> The extracts were subjected to PCR confirmation of bacterial identity under standard conditions (Tables S1–S3,† and 1).

**2.2.4. Determination of antibiotic resistant pattern.** For determination multidrug resistance (MDR) pattern of bacteria, twelve commonly used antibiotics, namely-Trimethoprim (COT-25), Cefuroxime (CXM-30), Cefotaxime (CTX-30), Cefixime (CFM-5), Linezolid (LZ-30), Kanamycin (K-30), Ciprofloxacin (CIP-5), Levofloxacin (LE-5), Erythromycin (E-15), Oxacillin (OX-30), Ampicillin (AMP-10), and Clindamycin (CD-2) (Table S3†) was performed following disk diffusion test.<sup>51</sup> The bacterial suspension was compared with 0.5 McFarland standard following CLSI guideline and spread over the entire surface of Mueller-Hinton (MH) agar medium by cotton swab.<sup>52</sup> The antimicrobial disks were placed on the MH agar and incubated at 37 °C temperature for overnight. After incubation the zone of inhibitions were measured to determine MDR pattern phenotypically (Fig. S1†). The phenotypically confirmed MDR bacteria were subjected to PCR detection of MDR genes (methicillin resistance *mecA* gene for *S. aureus*, beta-lactamase resistance *blaTEM-1*, and tetracycline resistance *tetA* genes for *E. coli*) for further confirmation of MDR bacteria.

**2.2.5. Antibiogram profiling of CuONPs against resistant bacteria.** The MDR isolates were spread on the freshly prepared MH agar, then CuONP-impregnated disks were placed over the inoculated medium and incubated overnight at 37 °C. The zone of inhibition surrounding the impregnated disks was determined as detailed above.

**2.2.6. MIC and MBC determination of CuONPs.** The Minimum Inhibitory Concentration (MIC) and Minimum Bactericidal Concentration (MBC) of CuONPs was determined following the standard broth dilution method and agar

diffusion method<sup>53</sup> against MDR isolates (Fig. S2†). Afterwards, turbidity was measured by calculating absorbance value using UV-Vis spectroscopy.<sup>3</sup> The lowest concentration of CuONPs that suppressed bacterial growth was considered the MIC, and the lowest concentration that completely inhibited bacterial growth was considered the MBC.

**2.2.7. Biosafety evaluation of CuONPs.** For biosafety evaluation, the viability of CuONP-treated BHK-21 cells was determined using MTT assay.<sup>54</sup>

**2.2.8. Cell culture and maintenance.** BHK-21 cells seeded from the frozen stock were thawed and installed in the cell culture plates at a density of  $0.4 \times 10^3$  cells per  $\text{cm}^2$  and maintained in a standard cell culture incubator providing all necessary nutrients (DMEM supplemented with 1% penicillin-streptomycin and 10% FBS) and maintained aseptically at 37 °C under 70% humidity and 5%  $\text{CO}_2$  for achieving a monolayer culture. The cells from the third passage were utilized for MTT assay.

**2.2.9. MTT assay of NP-treated cell.** MTT assay was performed according to Singh *et al.*<sup>54</sup> BHK-21 cells at a concentration of  $0.5 \times 10^5$  cells per well were seeded on a 96-well tissue culture plate and allowed to incubate at 37 °C while maintaining cell culture conditions. After 48 h, 80–90% of confluent cells were treated with various doses of NPs and cultured for another 24 h for evaluation of the effects of NPs. Then, 10  $\mu\text{l}$  of the MTT (3-(4,5-dimethylthiazol-2-yl)-2,5-diphenyltetrazolium bromide) stock solution ( $0.5 \text{ mg ml}^{-1}$ ) was added to each well and incubated for 4 h. Then the medium with MTT reagent was discarded and 100  $\mu\text{L}$  of DMSO was added into each well for 15 minutes to dissolve insoluble formazan. Finally, the plate was examined using an ELISA reader.

**2.2.10. Statistical analysis.** All values were expressed as mean  $\pm$  standard deviation, and all experiments were carried out in triplicate. Data were analyzed with one-way ANOVAs followed by paired *t*-tests using Origin 18 (Origin Lab, Northampton, MA, USA). Significant differences were evaluated at  $p < 0.05$  (\*) and  $p < 0.01$  (\*\*).

## 3. Results and discussion

### 3.1. Simplified synthesis of CuONPs

The green CuONPs synthesis approach used in this study employed copper sulphate pentahydrate ( $\text{CuSO}_4 \cdot 5\text{H}_2\text{O}$ ) as  $\text{Cu}^{2+}$  source and *Citrus limon* juice (citric acid) as reducing agent. The reaction conditions were empirically optimized for particle yield through several experiments. To this end, reaction parameters such as percentage of reducing agents, concentration of ion source, and period of reduction were altered. The formation of CuONPs was initially confirmed visually by observing changes in solution color, which is indicative of size-specific NP surface plasmon resonance and thus considered a primary indicator for the formation of NPs in the reaction solution.<sup>55</sup> When varying the reducing agent's concentration, a green color was achieved at 15% (Fig. 2a(ii)), whereas whitish, transparent, and light green solutions resulted from concentrations of 5%, 10%, and 20%, respectively (Fig. 2a(i), (ii), and (iv)). This concentration-based color shift appeared due to the alteration of ratio

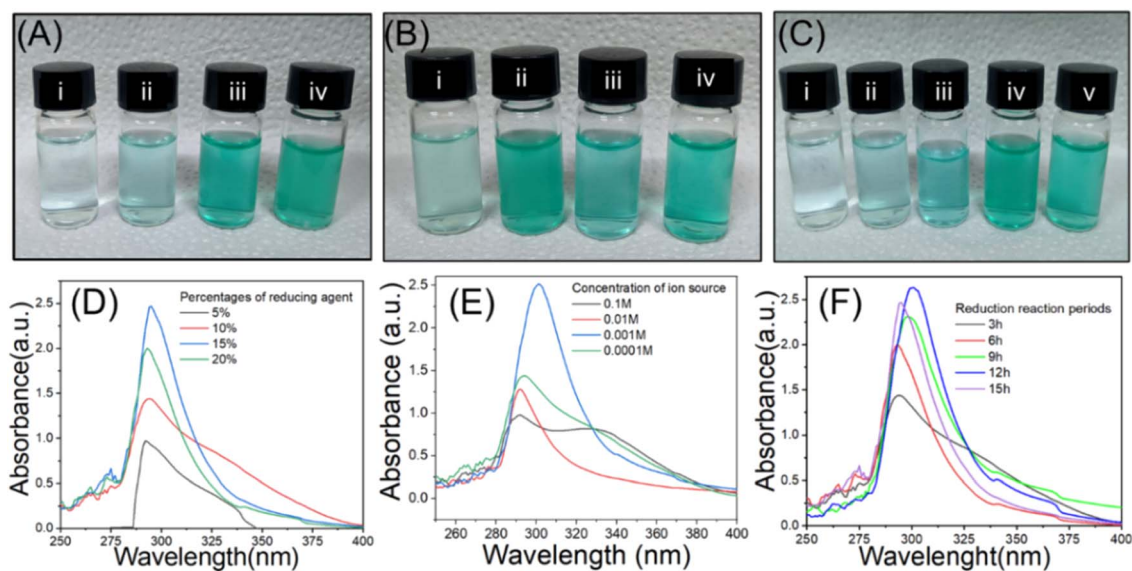


Fig. 2 Post-reduction solution color shift under (a) different concentrations of reducing agent (i. 5%; ii. 10%; iii. 15%; iv. 20%), (b) different concentrations of ion solution (i. 0.1 M; ii. 0.01 M; iii. 0.001 M; iv. 0.0001 M), and (c) different reduction reaction durations (i. 3 h; ii. 6 h; iii. 9 h; iv. 12 h; v. 15 h). (d–f) UV-visible absorption spectra for experiments (a–c), respectively.

between reducing agents and ion source.<sup>56</sup> The whitish to light green color shift was due to the presence of insufficient reducing agent for accomplishing the complete reduction of  $\text{Cu}^{2+}$  in the solution. When testing ion source different molarities, green color was obtained from 0.001 M  $\text{Cu}^{2+}$  solution (Fig. 2b(iii)), while transparent, deep green, and light green solutions resulted from molarities of 0.1 M, 0.01 M, and 0.0001 M, respectively (Fig. 2b(i), (ii), and (iv)). The green color solution indicated complete reduction of the  $\text{Cu}^{2+}$  at a suitable ratio of reducing agent and ion source,<sup>32</sup> while lighter color indicated incomplete reduction.<sup>57</sup> When testing time-based differences, green color was achieved after 12 h and 15 h of reduction (Fig. 2c(iv) and (v)), while whitish, transparent, and light green solutions resulted after 3 h, 6 h, and 9 h, respectively (Fig. 2c(i–iii)). As before, the lighter solutions indicated incomplete reduction. We thus concluded that an ion source of 0.001 M concentration combined with 15% reducing agent for 12 h represented suitable conditions for a maximum yield of CuONPs.

This visual observation was further verified by UV-Vis spectroscopic analysis of the specific absorption peak of CuONPs ( $\lambda_{\text{max}}$ ), which is at 280–320 nm.<sup>58</sup> Many previous studies have shown that absorption peak intensity was correlated with particle yield in such experiments.<sup>32,59</sup> We found that the maximum  $\lambda_{\text{max}}$  of 295 nm was present when using 15% reducing agent (Fig. 2d, blue line), while the other concentrations resulted in lesser absorption peaks and thus CuONP yields (Fig. 2d, other lines), thus validating the conclusion from the visual assessment. Similarly, the strongest absorption peak for different ion source molarities (295 nm) was present at 0.001 M (Fig. 2e, blue line), indicated maximum yield of CuONPs,<sup>60</sup> while other concentrations yielded weaker peaks at 315 nm. Such ion source concentration-based variation of  $\lambda_{\text{max}}$  peak has been reported in many previous studies.<sup>28,31,34,39,61</sup> Finally, the

strongest absorption peak among different reduction periods (295 nm) was found at 12 h (Fig. 2f, blue line), while the other reaction times yielded lower peaks. Again this correlation of reduction reaction period with particle yield has been previously reported for other nanoparticles.<sup>62</sup> In summary, UV-Vis analysis confirmed the visual assessment-based selection of optimal yield synthesis conditions of 15% reducing agent with a 0.001 M concentration of ion source and a 12 h reduction period. We then subjected the initially confirmed CuONPs to FTIR investigation to confirm the mechanism of NPs formation.

### 3.2. FTIR and XRD investigations of green CuONPs

The mechanism of CuONPs formation was investigated by observing chemical bond-specific vibrations at the respective resonant frequencies using FTIR (Fig. 3a and Table 2). The high spectral region at  $620\text{ cm}^{-1}$  intense broad band generated by Cu–O stretches in CuONPs during the reduction of  $\text{CuOS}_4 \cdot 5\text{H}_2\text{O}$ ,<sup>63</sup> as previously reported.<sup>64</sup> Another high spectral region at  $3360\text{ cm}^{-1}$  was generated by the formation of O–H bonds in all cases because the acidic hydroxyl groups surrounding the NPs act as capping agents.<sup>65</sup> These hydroxyl groups appeared after employing lemon juice as reducing agent.<sup>66</sup> The vibration bands at  $1657\text{ cm}^{-1}$  and  $1046\text{ cm}^{-1}$  are characteristic of the formation of C=O and C–O bonds, respectively in the CuO–citric acid complex, while the peak at  $2071\text{ cm}^{-1}$  derives the formation of C–H bonds, as previously reported.<sup>63</sup> These findings serve as elemental confirmation of CuONPs formation. This result indicated the nano formulated of bulk  $\text{CuOS}_4 \cdot 5\text{H}_2\text{O}$  was achieved through reducing with lemon juice.<sup>67</sup> In the case of lemon juice, the FTIR data revealed a strong peak at  $3290\text{ cm}^{-1}$  due to the presence of O–H group while the peaks  $1712\text{ cm}^{-1}$ ,  $1105\text{ cm}^{-1}$ , and  $778\text{ cm}^{-1}$  due to the presence of C=O, C–OH, and  $\text{CH}_2$ . Such peaks were appeared due to the presence of citric acid in the solution as described in many

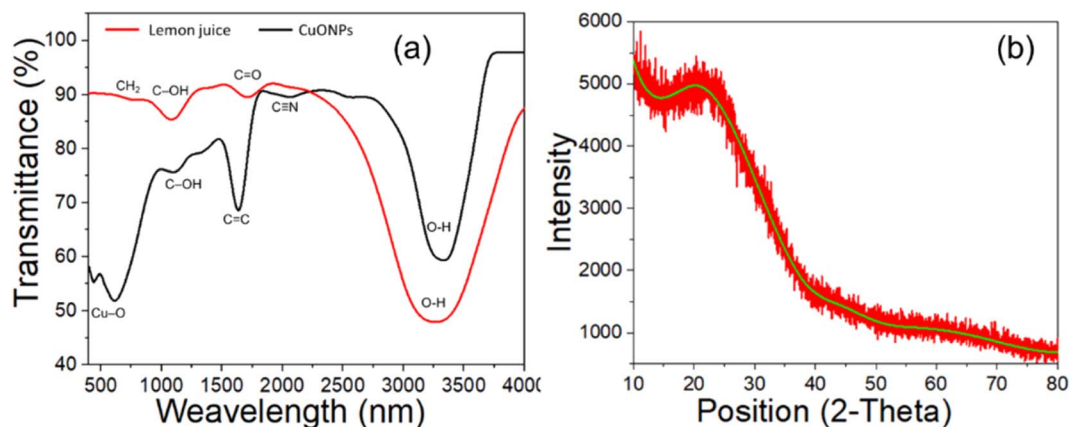


Fig. 3 FTIR spectra and XRD data obtained from lemon juice and green synthesized CuONPs using lemon juice as reducing agent.

Table 2 The FTIR stretching of different functional groups formed during synthesis of NPs and fresh lemon juice

Name of materials	Functional groups	Frequency (cm <sup>-1</sup> )	References
CuONPs	Cu-O	620	31,39,61,64,65
	O-H	3360	
	C=O	1657	
	C-O	1046	
	C-H	2071	
Lemon juice (citric acid)	O-H	3290	67,68
	C=O	1712	
	C-OH	1105	
	CH <sub>2</sub>	778	

previous research.<sup>67,68</sup> While other phytochemicals of the lemon juice, such as Sugar, Ascorbic acid, Malic acid *etc.* would have been involved with reduction of copper ion to form CuONPs.<sup>68</sup>

The CuONPs suffer from their amorphous nature which disabled the use X-ray crystallography to discuss the exact crystallinity of the of the yielded products.<sup>69</sup> The XRD pattern of the synthesized CuONPs depicted in Fig. 3b reveals its amorphous nature and the absence of crystalline phase. It means that like other polymerization approach of nanoparticle synthesis, this lemon juice based reduction method does not follow ideal crystallinity which often results in amorphous structure.<sup>70</sup>

### 3.3. AFM, SEM, TEM and DLS investigations of CuONPs

Three-dimensional (3D) topographic AFM images obtained from a surface spin coated with the yielded CuONPs were analyzed to determine the morphological features and dimensions of the particles. Surface roughness analysis revealed that NP formation was initiated at 3 h of reduction (Fig. 4a) and increase in particles continued until 12 h. Such increasing particle yield over the reduction period have been reported before.<sup>71</sup> The homogeneously dispersed CuONPs observed after

12 h constitute maximum particle yield (Fig. 4d) since the reduction reaction was complete. Lesser continued growth until 15 h (Fig. 4e) was caused by the aggregation of particles,<sup>3</sup> as previously described.<sup>3,72</sup> The control surface showed no such growth (Fig. 4f). Surface roughness analysis using AFM images revealed average particle dimensions of 92 nm × 155 nm at 12 h (Fig. 4g). A nonsignificant decrease ( $p > 0.05$ ) in height and width was observed between 12 h and 15 h, while the increase observed between 9 h and 12 h was highly significant. This reduction period-based size distribution of yielded particles was reported previously.<sup>3,73</sup> We therefore considered a reduction period of 12 h as the optimum duration for maximum yield of particles.

The yielded CuONPs were also drop-casted on a silicon wafer and subjected to SEM and TEM investigations. The SEM image analysis of yielded CuONPs drop-casted surface revealed round to spherical shaped with agglomerated NPs as shown in Fig. 4(i). The SEM has already been proven as a potential tool for determining the shape of the nanoparticles.<sup>58</sup> The TEM image analysis also revealed round to spherical shaped with agglomerated NPs as was revealed from SEM.<sup>69</sup> During the drop casting and curing of the CuONPs solution, nanoparticles tend to agglomerate and hence the larger size particles were revealed. While many non-agglomerated individual nanoparticles of around 150 nm were also realized from both the SEM and TEM images.<sup>74,75</sup> Besides, the spin coated sample for AFM analysis realized homogeneously dispersed without such agglomeration indicating that the nanoparticle will remain uniformly dispersed without agglomeration in liquid phase for obtaining the optimum effect for *in vitro* and *in vivo* antibacterial application.<sup>76</sup> This observation was further verified with the determination of average hydrodynamic size of CuONPs solution using DLS. The DLS spectrum revealed that homogenous populations of CuONPs dispersed in the solution without any agglomeration and the hydrodynamic size of synthesized CuONPs were ranges from 50.5 nm to 295 nm and the average particle size was 142.9 nm (Fig. 5). Such hydrodynamic size distribution of CuONPs were revealed from many previous studies.<sup>26,58,59</sup>

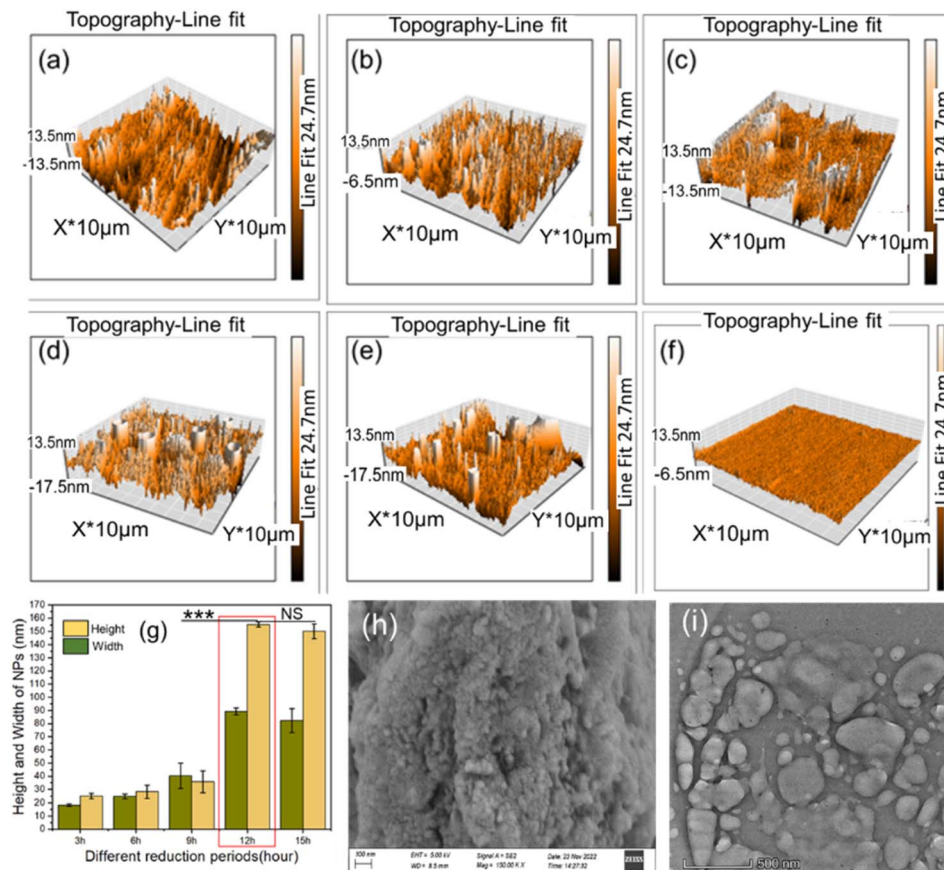


Fig. 4 Showed topographic and morphological images of CuONPs where three-dimensional AFM images of yielded CuONPs after reduction for (a) 3 h, (b) 6 h, (c) 9 h, (d) 12 h, and (e) 15 h, (f) control surface, (g) height and width profile of yielded CuONPs from AFM image, (h) SEM image of CuONPs after 12 h, and (i) TEM image of CuONPs after 12 h.

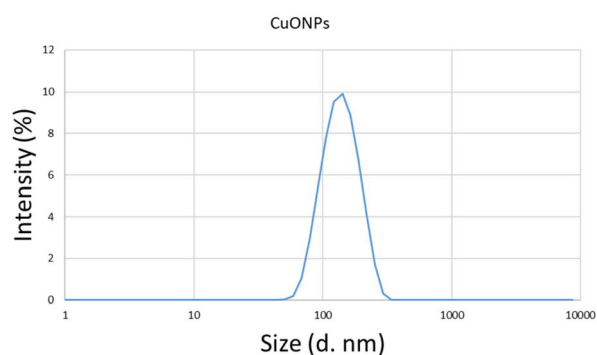


Fig. 5 The hydrodynamic size distribution spectrum of CuONPs using DLS.

#### 3.4. Identification and characterization of MDR-positive *S. aureus* and *E. coli*

For antibiogram profiling, multidrug-resistant (MDR) *S. aureus* and *E. coli* were collected from laboratory stock and reconfirmed following standard microbiological procedure<sup>77</sup> (culturing, gram staining, and PCR) (Fig. 6). The Gram-positive *S. aureus* was identified from yellow colonies on yellowish Mannitol Salt Agar plates (Fig. 6a), appearing as round purple

clusters with cocci arrangements under microscopic observation after Gram staining (Fig. 6b), and showing an amplified band at 228 bp for the *16srRNA* gene under PCR (Fig. 6c).<sup>3</sup> The Gram-negative *E. coli* were identified from round colonies with a metallic green sheen on eosinophil methylene blue agar (Fig. 6d), large pink cells with a rod-shaped structure under microscopic observation (Fig. 6e), and presence of a PCR-amplified band at 585 bp for the *malB* gene (Fig. 6f).<sup>78</sup> The PCR confirmed *S. aureus* and *E. coli* were then subjected to determination of MDR genes.

#### 3.5. Determination of multidrug resistance gene

The multidrug resistance (MDR) pattern of PCR-confirmed *S. aureus* and *E. coli* was investigated both phenotypically by antibiogram assay and genotypically by PCR test of MDR genes. Based on the zone of inhibition surrounding the disks, both *S. aureus* and *E. coli* were resistant to six groups of antibiotics: cephalosporins, sulfonamides, oxazolidinone, macrolides, penicillin, and lincosamides (Table S4, Fig. S1a and b†), indicating that both isolates were MDR (*i.e.*, resistant to more than three antibiotics classes).<sup>79</sup> These phenotypically confirmed MDR isolates were further subjected to PCR analysis to detect the methicillin resistance gene *mecA* of *S. aureus* and the beta-lactamase resistance gene *blaTEM-1* and tetracycline

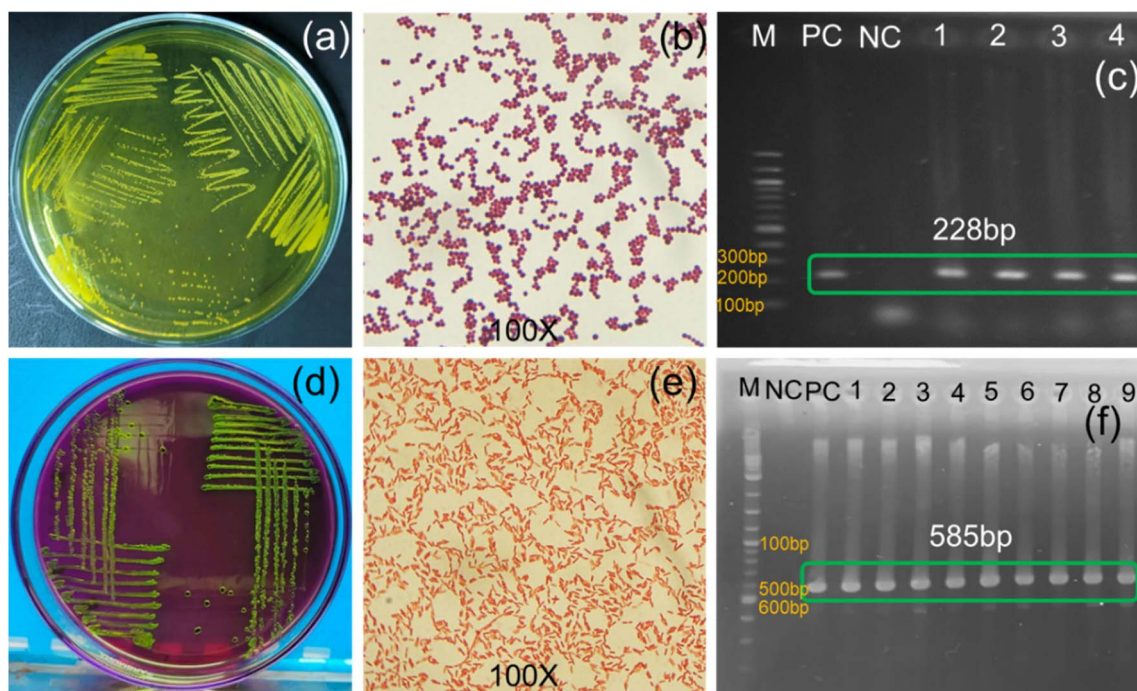


Fig. 6 Cultural, morphological, and molecular characterization of *S. aureus*: (a) yellow colony on MSA, (b) purple cocci, (c) 228 bp band for the *16s rRNA* gene. For *E. coli*: (d) round colonies with metallic green sheen on EMB, (e) pink, rod-shaped cells, and (f) 585 bp band for the *malB* gene.

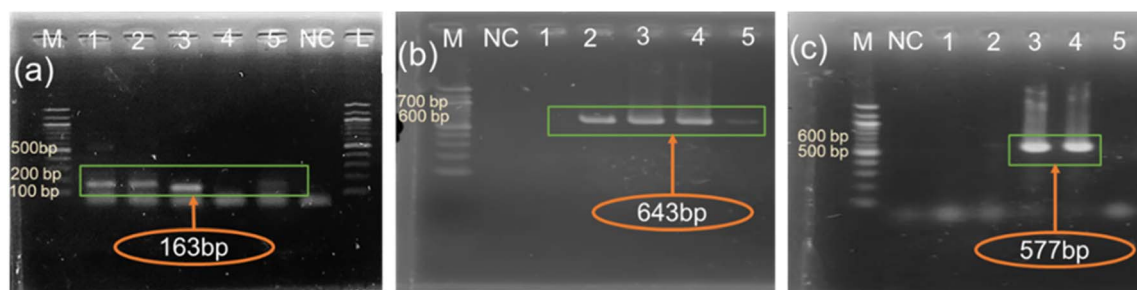


Fig. 7 PCR-amplified bands of (a) 163 bp for methicillin resistance gene *mecA*, (b) 643 bp for the beta-lactamase resistance gene *blaTEM-1*, and (c) 577 bp for the tetracycline resistance gene *tetA*.

resistance gene *tetA* of *E. coli* (Fig. 7). The amplified band at 163 bp for *mecA* (Fig. 7a) indicates the presence of methicillin-resistant *S. aureus*,<sup>47</sup> as confirmed previously.<sup>80,81</sup> The amplified bands at 643 bp and 577 bp for *blaTEM-1* (Fig. 7b) and *tetA* (Fig. 7c) indicate beta-lactamase and tetracycline resistance in *E. coli*, as reported previously.<sup>82,83</sup> These MDR confirmed isolates were then subjected to antibacterial evaluation using the disk diffusion method,<sup>77</sup> with the aim of interpreting the zone of inhibition of caused by CuONPs.

### 3.6. Antibacterial activity of yielded CuONPs

The zones of inhibition of disks impregnated with CuONPs synthesized under different reduction conditions were measured to evaluate their antibacterial activity against MDR bacteria (Fig. S2†). For reducing agent concentration, the maximum zone of inhibition ( $18 \pm 0.8$  mm) was found for the 15% reducing agent treatment (Fig. S2a†) while significantly

smaller zones of inhibition appeared for lower reducing agent concentrations ( $14 \pm 0.3$  mm,  $16 \pm 0.2$  mm, and  $17 \pm 0.7$  mm for 5%, 10%, 20% reducing agent, respectively), a correlation of reducing agent concentration to inhibition zone size was previously observed.<sup>3,84</sup> A significantly ( $p \leq 0.001$ ) greater zone of inhibition ( $20 \pm 0.8$  mm) was found for ciprofloxacin (positive control) (Fig. S2a and d†). For the treatments with variable ion source concentrations, the maximum zone of inhibition ( $26 \pm 0.1$  mm) appeared at 0.001 M (Fig. S2b†), while significantly ( $p \leq 0.01$ ) smaller zones were found for the other treatments ( $16 \pm 0.2$  mm,  $21 \pm 0.5$  mm, and  $17 \pm 0.2$  mm for 0.1 M, 0.01 M, and 0.0001 M, respectively) and for positive control ( $23 \pm 0.4$ ) (Fig. S2b and e†), a response that has been previously demonstrated.<sup>3,85</sup> Finally, among different reduction periods, the maximum zone of inhibition ( $26 \pm 0.5$  mm) was present for the 12 h treatment (Fig. S2c†), while significantly ( $p \leq 0.01$ ) smaller zones were found for the other treatment durations ( $19 \pm 0.5$



Table 3 Comparative performance of the antibacterial activity of CuONPs synthesized with different conditions

Use of reducing agents	Evaluation pattern against MDR bacteria	The source of bacteria investigated	Name of organisms	Doses of NPs ( $\mu\text{g ml}^{-1}$ )		Zone of inhibition (mm)/growth of bacteria	References
				MIC	MBC		
<i>Gloriosa superba</i> L. extract	Not done	Laboratory stock	1. <i>Klebsiella aerogenes</i> 2. <i>Escherichia coli</i> 3. <i>Staphylococcus aureus</i> 4. <i>Pseudomonas desmolyticum</i>	100	—	12.00 $\pm$ 0.00 7.33 $\pm$ 0.33 3.33 $\pm$ 0.33 2.67 $\pm$ 0.33	33
<i>Morinda tinctoria</i>	Not done	Unknown	1. <i>S. aureus</i> 2. <i>B. subtilis</i> 3. <i>E. coli</i> 4. <i>P. aeruginosa</i>	500	1000	10 16 12 10	61
<i>Acanthospermum hispidum</i> L. leaves extract	Not done	Human pathogen	1. <i>E. coli</i> 2. <i>P. aeruginosa</i> 3. <i>S. pyogenus</i> 4. <i>S. aureus</i>	25 50 100 250	—	13 12 17 18	87
Gum karaya	Not done	Laboratory stock	1. <i>E. coli</i> 2. <i>S. aureus</i>	103 $\pm$ 4.7 120 $\pm$ 8.1	125 $\pm$ 5.5 135 $\pm$ 8.8	16.2 $\pm$ 0.8 14.5 $\pm$ 0.6	88
<i>Aerva javanica</i> leaf extract	Not done	Laboratory stock	1. <i>E. coli</i> 2. <i>P. aeruginosa</i> 3. <i>S. aureus</i> 4. <i>Acinetobacter</i>	128	128	6 $\pm$ 1 10 $\pm$ 1 12 $\pm$ 1 12 $\pm$ 1	64
<i>Citrus limon</i>	Not done	Laboratory stock	1. <i>S. aureus</i> 2. <i>E. coli</i>	N/A	—	20 25	64
<i>Bifurcaria bifurcate</i> extract	Not done	Laboratory stock	1. <i>Enterobacter aerogenes</i> 2. <i>S. aureus</i>	20	—	14 16	55
<i>Justicia gendarussa</i>	Not done	Laboratory stock	1. <i>E. coli</i> 2. <i>S. aureus</i>	75	—	16 18	58
<i>Citrus limon</i>	Done	Laboratory stock	1. <i>S. aureus</i> 2. <i>E. coli</i>	0.8 1.6	1.6 3.1	26 $\pm$ 0.5 24 $\pm$ 0.1	This study

mm, 20  $\pm$  0.5 mm, and 23  $\pm$  0.1 mm for 6 h, 9 h, 15 h, respectively) and control (24  $\pm$  0.1 mm) (Fig S2c and f†), which agreed with previous results.<sup>3,86</sup> We therefore conclude that 15% reducing agent with a 0.001 M concentration of ion source and a 12 h reduction reaction period considered as optimum conditions for yielding maximum CuONPs. Additionally, the green synthesized CuONPs found superior to other previously synthesized nanoparticles in terms of zone of inhibition, MIC and MBC value and effectiveness against MDR bacteria as shown in the Table 3.

The antibiogram result revealed that, CuONPs showed 18  $\pm$  96 mm, 19  $\pm$  98 mm, and 18  $\pm$  98 mm sensitive zones of inhibition against methicillin resistant *S. aureus* (Fig. 8a), beta-lactamase resistant (*blaTEM-1*) *E. coli* (Fig. 8b), and tetracycline resistant (*tetA*) *E. coli* (Fig. 8c) respectively. While such zone of inhibitions was absence when only lemon juice (15% lemon juice, as use for reduction) and bulk Copper salt (0.001 M  $\text{CuSO}_4 \cdot 5\text{H}_2\text{O}$ , as use for iron source) solution was employed against all those resistant isolates. In case of positive control (Amikacin), the sensitive zones of inhibition appeared showing

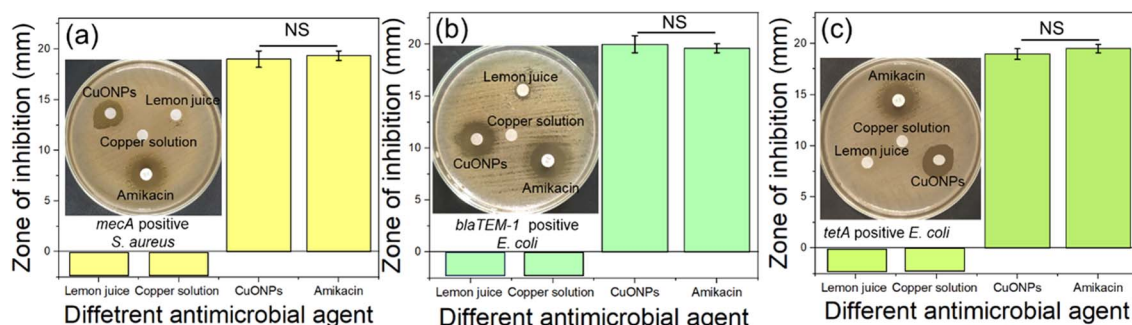


Fig. 8 Antibacterial effect evaluation of CuONPs against (a) methicillin (*mecA*) resistant *S. aureus*, (b) beta-lactamase resistant (*blaTEM-1*) *E. coli*, and (c) tetracycline resistant (*tetA*) *E. coli*.

nonsignificant difference with the yielded CuONPs indicating the effectiveness of the yielded particle against MDR bacteria. Besides, the absence of zone of inhibition surrounding the lemon juice and bulk Copper salt solution indicated that the sensitive zone of inhibition appeared after their nano-formulation. Thus, the green synthesized CuONPs proved to be effective against bacteria irrespective of their antibiotic resistance.

The synthesized CuONPs with enhanced antibacterial activity were also subjected to determination of MIC and MBC by spectrochemical analysis of the optical density (OD) of bacteria-inoculated cultured broth treated with various concentrations of NPs (Fig. 9). OD <0.06–0.07 was considered as

representing an inhibitory concentration.<sup>89</sup> The complete inhibition of MDR-positive *E. coli* growth was observed at  $2^{-5}$  dilution with a MIC of  $1.6 \mu\text{g ml}^{-1}$ , while the complete inhibition of MDR *S. aureus* was observed at  $2^{-6}$  dilution with a MIC of  $0.8 \mu\text{g ml}^{-1}$  (Fig. 9a). The MBC of CuONPs was determined by counting colony-forming units (CFUs) according to agar diffusion methods,<sup>85</sup> where a CFU <30 was considered as the minimum bactericidal concentration.<sup>85</sup> A bactericidal effect of CuONPs against MDR *E. coli* was observed at  $2^{-4}$  dilution (Fig. S3b†) with MBC  $3.1 \mu\text{g ml}^{-1}$ , while that for MDR *S. aureus* was observed at  $2^{-5}$  dilution (Fig. S3a†) with MBC  $1.6 \mu\text{g ml}^{-1}$  (Fig. 9b). Finally, we confirmed that dose of  $8 \mu\text{g ml}^{-1}$  of CuONPs functioned as the bactericidal concentration for broad-spectrum application.

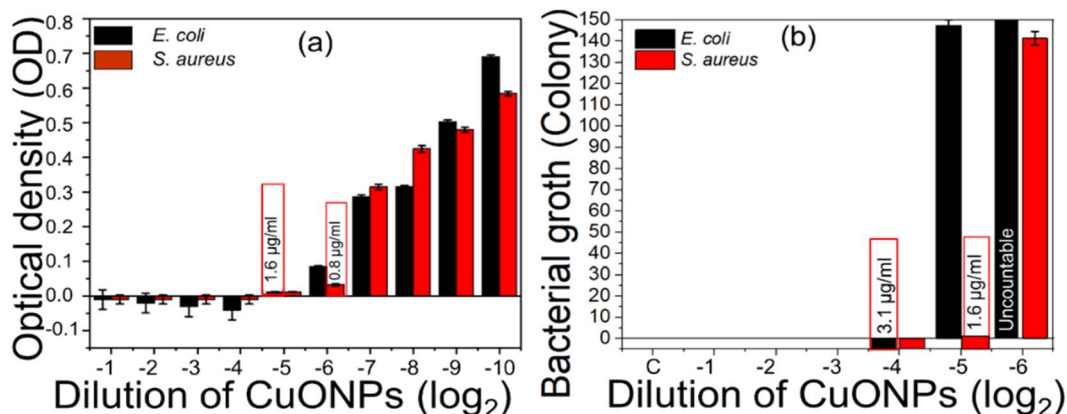


Fig. 9 (a) MIC and (b) MBC of CuONPs against MDR *E. coli* and *S. aureus*.

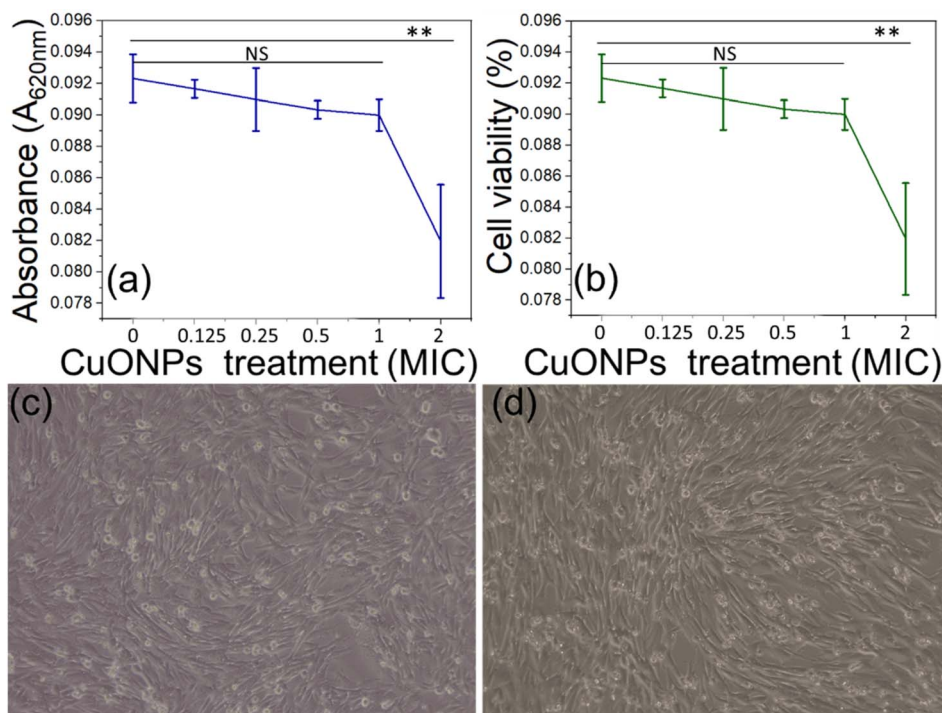


Fig. 10 MTT assay of CuONPs using ELISA reader. (a) OD of CuONP-treated cells, (b) cell viability assay of CuONP-treated cells, (c) control BHK-21 cells at 72 h post seeding, and (d) CuONP-treated cells at 24 h post treatment.

This indicates that the yielded CuONPs can be considered as better antibacterial agents than previously synthesized CuONPs (Table 3), which also were not bio-compatible due to the use of chemical reducing agents.<sup>90</sup> Previous attempts to address this issue using natural extracts as reducing agents still required large doses because most of the synthesis protocols employed additional capping agents which often inhibit exposure of the functional groups of NPs during antibacterial activity.<sup>40</sup> The simplified synthesis employed here, using only lemon juice as reducing agent, produced enhanced antibacterial effects with low MIC and MBC doses against MDR bacteria because most of the functional groups of NPs were open and effective. Similarly, while excellent antibacterial effects against normal *S. aureus* and *E. coli* were previously demonstrated<sup>3,44</sup> (Table 3), comparable effectivity against MDR bacteria yet remains to be shown. MDR bacteria are increasingly regarded as a major challenge because mechanisms required for their inhibition are totally different than for normal bacteria. Considering their resistance patterns, this study used MDR *S. aureus* and *E. coli* for evaluating the antibacterial performance of yielded NPs (Table 3). Overall, we here have demonstrated that our synthesis program is simple to implement, ecologically friendly, and biocompatible for use of controlling MDR bacteria in the environment.

### 3.7. Biosafety evaluation of CuONPs

The biosafety compliance of any therapeutic substance is considered as crucial step prior to its *in vivo* application. We performed biosafety evaluation of CuONPs using the BHK-21 cell line (Fig. 10a and b) by measuring mitochondrial reductase enzyme activity in a colorimetric MTT assay.<sup>91</sup> In principle, the mitochondrial reductase enzyme of any healthy living cell reduces MTT reagent (3-(4,5-dimethylthiazol-2-yl)-2,5-diphenyltetrazolium Bromide) to form insoluble formazan, and upon hydrolysis with DMSO this produces a coloured solution.<sup>91</sup> Measuring this color by its OD allows monitoring cell health status.<sup>92</sup> Colorimetric biosafety assessment showed a nonsignificant ( $0.01 < p \leq 0.05$ ) difference in cell viability and OD value between the control and cells treated with NP doses of  $\sim$ MIC (Fig. 10c and d), whereas significant differences were present at double MIC dose. In the latter case, cell viability was decreased due to the changes in pH of the cell-containing medium because of the presence of citric acid,<sup>93</sup> this is because we employed the yielded CuONPs in a solution containing unused citric acid. However, lyophilized CuONPs from the yielded solution could sidestep this issue of pH-based viability decrease. We therefore conclude that the CuONPs created by our process can be regarded as biocompatible for any therapeutic *in vivo* applications.

## 4. Conclusions

This green synthesis program successfully synthesized CuONPs employing  $\text{CuSO}_4 \cdot 5\text{H}_2\text{O}$  solution as ion the source and *citrus lemon* juice as reducing as well as capping agent for antibacterial application against MDR bacteria. The particle yield was confirmed primarily by UV. Vis analysis and the particles yield,

size distribution, elemental confirmation, and other morphological features were confirmed by AFM, SEM, TEM, DLS, FTIR, XRD *etc.* Most of the physical investigations demonstrated the maximum yield of NPs from a 0.001 M ion source by reducing with 15% reducing agent over 12 h. The yielded CuONPs showed effective antibacterial effects against both methicillin-resistant (*mecA*-positive) *S. aureus* (Gram-positive) and beta-lactamase- (*bla*<sub>TEM-1</sub>-positive) and tetracycline-resistant (*tetA*-positive) *E. coli* (Gram-negative). The antibacterial effects of the yielded CuONPs showed superior to other previously synthesized nanoparticles in terms of maximum zone of inhibition, MIC and MBC values. These results suggest that the yielded particles can be used in broad-spectrum applications against both Gram-positive and Gram-negative bacteria irrespective of their resistance patterns. Although double MIC doses showed pH change-based effects on cellular viability, dosage at MIC level did not significantly affect the mammalian cell system, indicating that the synthesized CuONPs are biocompatible for *in vivo* applications. We therefore suggest that CuONPs generated by our approach can be applied in poultry farms for safely controlling environmental MDR bacteria.

## Author contributions

A. R. and A. R.: work, write, data analysis and formatted of the manuscript. S. A.: work to this research. N. Y., G. K. D, T. H., and K. S. H.: performed physical characterization of FTIR and AFM. T. F.: performed TEM, XRD, and DLS characterization of NPs. M. A. K.: conceptualization, supervision for the research activities, design methodology, data curation, funding, resources, verification of data, writing of the original draft and writing and editing of the manuscript; M. T. H.: supervision for the research activities, data analysis and verification of data. J. W. C.: supervision, data curation, funding, resources, verification of data, writing and editing of the manuscript; All authors reviewed the final manuscript. All authors consent to publish.

## Conflicts of interest

The authors declare no conflict of interest.

## Acknowledgements

This research was supported by the project “Development of chitosan graphene based nanobiosensor for curving buffalo mortality through early-stage detection of HS (Project. No. 2022/1603/BLRI)”, an outsourcing project of Buffalo Research and Development Project, Bangladesh Livestock Research Institute (BLRI), by International Science Program, Uppsala University, Sweden and National Research Foundation of Korea (NRF) grant funded by the Korea government (MSIT) (No. 2019R1A2C3002300), by the National R&D Program through the NRF funded by Ministry of Science and ICT (NRF-2022M3H4A1A01005271), by GRDC Cooperative Hub through the National Research Foundation of Korea funded by the Ministry of Science and ICT (Grant number RS-2023-00259341).

## References

- 1 W. Gao and L. Zhang, *Nat. Rev. Microbiol.*, 2021, **19**, 5–6.
- 2 C. Manyi-Loh, S. Mamphweli, E. Meyer and A. Okoh, Antibiotic use in agriculture and its consequential resistance in environmental sources: Potential public health implications, *Molecules*, 2018, **23**, 795.
- 3 A. Rahman, H. Rasid, I. Ali, N. Yeachin, S. Alam, K. S. Hossain and A. Kaf, *J. Nanotechnol.*, 2023, **2023**, 1–18.
- 4 T. M. Uddin, A. J. Chakraborty, A. Khusro, B. R. M. Zidan, S. Mitra, T. Bin Emran, K. Dhama, M. K. H. Ripon, M. Gajdacs, M. U. K. Sahibzada, M. J. Hossain and N. Koirala, *J. Infect. Public Health*, 2021, **14**, 1750–1766.
- 5 V. Economou and P. Gousia, *Infect. Drug Resist.*, 2015, **8**, 49–61.
- 6 M. A. Nnorom, D. Saroj, L. Avery, R. Hough and B. Guo, *J. Hazard. Mater.*, 2023, **446**, 130628.
- 7 R. Abreu, T. Semedo-lemsaddek and E. Cunha, *Microorganisms*, 2023, **11**, 1–35.
- 8 K. Koutsoumanis, A. Allende, A. Álvarez-Ordóñez, D. Bolton, S. Bover-Cid, M. Chemaly, R. Davies, A. De Cesare, L. Herman, F. Hilbert, R. Lindqvist, M. Nauta, G. Ru, M. Simmons, P. Skandamis, E. Suffredini, H. Argüello, T. Berendonk, L. M. Cavaco, W. Gaze, H. Schmitt, E. Topp, B. Guerra, E. Liébana, P. Stella and L. Peixe, *EFSA J.*, 2021, **19**, e06651.
- 9 W. Wang, M. I. Arshad, M. Khurshid, M. H. Rasool, M. A. Nisar, M. A. Aslam and M. U. Qamar, *Infect. Drug Resist.*, 2018, **11**, 1645–1658.
- 10 H. D. Hedman, K. A. Vasco and L. Zhang, *Animals*, 2020, **10**, 1–39.
- 11 M. Z. Hosain, S. M. Lutful Kabir and M. M. Kamal, *Vet. World*, 2021, **14**, 210–221.
- 12 M. M. Hassan, M. E. El Zowalaty, Å. Lundkvist, J. D. Järhult, M. R. Khan Nayem, A. Z. Tanzin, M. R. Badsha, S. A. Khan and H. M. Ashour, *Trends Food Sci. Technol.*, 2021, **111**, 141–150.
- 13 R. Khatun, A. Jabbar Howlader, S. Ahmed, N. Islam, K. Alam, S. Haider, M. Showkat Mahmud and M. A. Hasan, *Univers. J. Public Health*, 2018, **6**, 14–22.
- 14 T. Shafiq, M. Uzair, M. J. Iqbal, M. Zafar, S. J. Hussain and S. A. A. Shah, *Nano Biomed. Eng.*, 2021, **13**, 191–206.
- 15 S. S. Salem, *Arch. Microbiol.*, 2023, **205**, 1–15.
- 16 S. S. Salem, E. N. Hammad, A. A. Mohamed and W. El-Dougdoug, *Biointerface Res. Appl. Chem.*, 2023, **13**, 41.
- 17 S. Dawadi, S. Katuwal, A. Gupta, U. Lamichhane, R. Thapa, S. Jaisi, G. Lamichhane, D. P. Bhattarai and N. Parajuli, *J. Nanomater.*, 2021, **2021**, 6687290.
- 18 M. Golbashy, H. Sabahi, I. Allahdadi, H. Nazokdast and M. Hosseini, *Arch. Agron. Soil Sci.*, 2017, **63**, 84–95.
- 19 K. Priya and A. K. Sidhu, *Front. Nanotechnol.*, 2021, **3**, 655062.
- 20 L. Benhalima, S. Amri, M. Bensouilah and R. Ouzrout, *Pakistan J. Med. Sci.*, 2019, **35**, 1322–1328.
- 21 T. Gomes, P. Pinheiro, I. Cancio, C. G. Pereira and M. J. Bebianno, *Environ. Sci. Technol.*, 2011, **45**, 9356–9362.
- 22 M. B. Gawande, A. Goswami, T. Asefa, X. Huang, R. Silva, X. Zou, R. Zboril and R. S. Varma, *Chem. Rev.*, 2016, **116**, 3722–3811.
- 23 S. N. M. Yusoff, A. Kamari and N. F. A. Aljafree, *Int. J. Environ. Sci. Technol.*, 2016, **13**, 2977–2994.
- 24 A. Rahman, K. J. Roy, K. M. A. Rahman, M. K. Aktar, M. A. Kafi, M. S. Islam, M. B. Rahman, M. R. Islam, K. S. Hossain, M. M. Rahman and H. Heidari, *Nano Sel.*, 2021, **3**, 188–200.
- 25 M. Rani Sarkar, M. H. or Rashid, A. Rahman, M. A. Kafi, M. I. Hosen, M. S. Rahman and M. N. Khan, *Environ. Nanotechnol. Monit. Manag.*, 2022, **18**, 100687.
- 26 S. Naz, A. Gul, M. Zia and R. Javed, *Appl. Microbiol. Biotechnol.*, 2023, **107**, 1039–1061.
- 27 S. E. D. Hassan, A. Fouda, A. A. Radwan, S. S. Salem, M. G. Barghoth, M. A. Awad, A. M. Abdo and M. S. El-Gamal, *J. Biol. Inorg. Chem.*, 2019, **24**, 377–393.
- 28 A. A. Badawy, N. A. H. Abdelfattah, S. S. Salem, M. F. Awad and A. Fouda, *Biology (Basel)*, 2021, **10**, 1–20.
- 29 S. Moniri Javadhesari, S. Alipour, S. Mohammadnejad and M. R. Akbarpour, *Mater. Sci. Eng. C*, 2019, **105**, 110011.
- 30 S. Shirsat, D. Pawar, N. Jain, J. Pawar, V. S. Tale and R. Henry, *Asian J. Pharm. Clin. Res.*, 2019, **12**, 135–138.
- 31 B. Nahar, S. B. Chaity, M. A. Gafur and M. Z. Hossain, *J. Nanomater.*, 2023, **2023**, 2892081.
- 32 W. W. Andualem, F. K. Sabir, E. T. Mohammed, H. H. Belay and B. A. Gonfa, *J. Nanobiotechnol.*, 2020, **2020**, 2932434.
- 33 H. R. Naika, K. Lingaraju, K. Manjunath, D. Kumar, G. Nagaraju, D. Suresh and H. Nagabhushana, *J. Taibah Univ. Sci.*, 2015, **9**, 7–12.
- 34 R. Chopra, N. Kashyap, K. Amit and D. Banerjee, *Int. J. Eng. Res.*, 2020, **V9**, 258–261.
- 35 R. Zarzuela, I. Moreno-Garrido, J. Blasco, M. L. A. Gil and M. J. Mosquera, *Constr. Build. Mater.*, 2018, **187**, 501–509.
- 36 B. E. El Bialy, R. A. Hamouda, M. A. A. Eldaim, S. S. El Ballal, H. S. Heikal, H. K. Khalifa and W. N. Hozzein, *Int. J. Nanomed.*, 2020, **15**, 3827–3842.
- 37 K. F. Buazar, S. Sweidi and M. Badri, *Green Process. Synth.*, 2019, **8**, 691–702.
- 38 M. He, J. Zhang, H. Wang, Y. Kong, Y. Xiao and W. Xu, *Nanoscale Res. Lett.*, 2018, **13**, 1–7.
- 39 H. Veisi, B. Karmakar, T. Tamoradi, S. Hemmati, M. Hekmati and M. Hamelian, *Sci. Rep.*, 2021, **11**, 1–13.
- 40 A. K. Sidhu, N. Verma and P. Kaushal, *Front. Nanotechnol.*, 2022, **3**, 1–17.
- 41 D. Slimane Ben Ali, F. Krid, M. Nacef, E. H. Boussaha, M. L. Chelaghmia, H. Tabet, R. Selaimia, A. Atamnia and A. M. Affoune, *RSC Adv.*, 2023, **13**, 18734–18747.
- 42 T. I. Shaheen, A. Fouda and S. S. Salem, *Ind. Eng. Chem. Res.*, 2021, **60**, 1553–1563.
- 43 I. Khaldari, M. R. Naghavi and E. Motamedi, *RSC Adv.*, 2021, **11**, 3346–3353.
- 44 K. J. Roy, A. Rahman, K. Hossain and B. Rahman, *Appl. Microbiol. Open Access*, 2020, **6**, 173–183.
- 45 N. Rohland and M. Hofreiter, *Biotechniques*, 2007, **42**, 343–352.

- 46 S. R. Monday and G. A. Bohach, *J. Clin. Microbiol.*, 1999, **37**, 3411–3414.
- 47 M. Mehrotra, G. Wang and W. M. Johnson, *J. Clin. Microbiol.*, 2000, **38**, 1032–1035.
- 48 X. Jiang, R. Wang, Y. Wang, X. Su, Y. Ying, J. Wang and Y. Li, *Biosens. Bioelectron.*, 2011, **29**, 23–28.
- 49 X. T. Li, L. C. Thomason, J. A. Sawitzke, N. Costantino and D. L. Court, *Nucleic Acids Res.*, 2013, **41**, 1–8.
- 50 R. S. Kurnia, A. Indrawati, N. Luh, P. Ika and A. Priadi, *Vet. World*, 2018, **11**, 1581–1586.
- 51 N. Phiri, G. Mainda, M. Mukuma, N. N. Sinyangwe, L. J. Banda, G. Kwenda, E. M. Muonga, B. N. Flavien, M. Mwansa, K. Yamba, M. Munyeme and J. B. Muma, *J. Epidemiol. Res.*, 2020, **6**, 13.
- 52 A. L. Dolinsky, *M100 Performance Standards for Antimicrobial Susceptibility Testing*, 2017, vol. 8.
- 53 I. O. Chikezie, *Afr. J. Microbiol. Res.*, 2017, **11**, 977–980.
- 54 G. Singh, J. Beddow, C. Mee, L. Maryniak, E. M. Joyce and T. J. Mason, *Int. J. Toxicol.*, 2017, **36**, 478–484.
- 55 Y. Abboud, T. Saffaj, A. Chagraoui, A. El Bouari, K. Brouzi, O. Tanane and B. Ihssane, *Appl. Nanosci.*, 2014, **2014**, 571–576.
- 56 A. Benhammada and D. Trache, *J. Therm. Anal. Calorim.*, 2022, **147**, 1–16.
- 57 A. Bukhari, I. Ijaz, E. Gilani, A. Nazir, H. Zain, R. Saeed, S. S. Alarfaji, S. Hussain, R. Aftab and Y. Naseer, *Coating*, 2021, **11**, 1374.
- 58 S. Vasantharaj, P. Shivakumar, S. Sathiyavimal and P. Senthilkumar, *Appl. Nanosci.*, 2023, **13**, 2295–2302.
- 59 K. Velsankar, V. Vinothini, S. Sudhakar, M. K. Kumar and S. Mohandoss, *Appl. Nanosci.*, 2020, **10**, 3953–3971.
- 60 K. S. Siddiqi and A. Husen, *Biomater. Res.*, 2020, **24**, 11.
- 61 R. Radhakrishnan, F. Liakath, A. Khan and A. Muthu, *Lett. Appl. NanoBioScience*, 2021, **10**, 2706–2714.
- 62 K. Vishveshvar, M. V. A. Krishnan, K. Haribabu and S. Vishnuprasad, *BioNanoScience*, 2018, **8**, 554–558.
- 63 H. Karkehabadi, A. Rahmati, R. Abbasi, A. Farmany and R. Najafi, *BMC Oral Health*, 2023, **23**, 1–12.
- 64 F. Amin, B. Khattak, A. Alotaibi, M. Qasim, I. Ahmad, R. Ullah, M. Bourhia, A. Gul, S. Zahoor and R. Ahmad, *J. Evidence-Based Complementary Altern. Med.*, 2021, **2021**, 1–12.
- 65 M. Elango, M. Deepa, R. Subramanian and A. M. Musthafa, *Polym.-Plast. Technol. Eng.*, 2017, **0**, 1–12.
- 66 H. Qamar, S. Rehman, D. K. Chauhan, A. K. Tiwari and V. Upmanyu, *Int. J. Nanomed.*, 2020, **15**, 2541–2553.
- 67 M. Mahiuddin and B. Ochiai, *RSC Adv.*, 2021, **11**, 26683–26686.
- 68 P. Pimpang, R. Sumang and S. Choopun, *Chiang Mai J. Sci.*, 2018, **45**, 2005–2014.
- 69 M. A. A.-A. Mohammadikish, *Mater. Res. Express*, 2019, **6**, 045013.
- 70 M. Oh and C. A. Mirkin, *Nature*, 2005, **438**, 651–654.
- 71 N. T. K. Thanh, N. Maclean and S. Mahiddine, *Chem. Rev.*, 2014, **3**, 7610–7630.
- 72 E. Y. Shaba, J. O. Jacob, J. O. Tijani and M. A. T. Suleiman, *Appl. Water Sci.*, 2021, **11**, 48.
- 73 N. V. Notash, M. M. Heravi, A. Alhampour and P. Mohammadi, *Sci. Rep.*, 2020, 1–9.
- 74 M. S. Gorji, K. A. Razak and K. Y. Cheong, *Adv. Mater. Res.*, 2014, **1024**, 124–127.
- 75 S. Ikawa, K. Kitano and S. Hamaguchi, *Plasma Processes Polym.*, 2010, **7**, 33–42.
- 76 A. N. Nguyen, J. Solard, H. T. T. Nong, C. Ben Osman, A. Gomez, V. Bockelée, S. Tencé-Girault, F. Schoenstein, M. Simón-Sorbed, A. E. Carrillo and S. Mercone, *Materials (Basel)*, 2020, **13**, 1–18.
- 77 S. Akter, A. A. M. Sabuj, Z. F. Haque, M. T. Rahman, M. A. Kafi and S. Saha, *Vet. World*, 2020, **13**, 266–274.
- 78 X. Jiang, R. Wang, Y. Wang, X. Su, Y. Ying, J. Wang and Y. Li, *Biosens. Bioelectron.*, 2011, **29**, 23–28.
- 79 A. Wolfensberger, S. P. Kuster, M. Marchesi, R. Zbinden and M. Hombach, *Antimicrob. Resist. Infect. Control*, 2019, **3**, 1–9.
- 80 V. Rajan, G. K. Sivaraman, A. Vijayan, R. Elangovan, A. Prendiville and T. T. Bachmann, *Environ. Microbiol. Rep.*, 2022, **14**, 391–399.
- 81 E. Pyzik, A. Marek, D. Stępień-Pyśniak, R. Urban-Chmiel, L. S. Jarosz and I. Jagiełło-Podębska, *J. Vet. Res.*, 2019, **63**, 183–190.
- 82 M. A. Saeed, A. Haque, A. Ali, M. Mohsin, S. Bashir and A. Tariq, *J. Antibiot. (Tokyo)*, 2009, **62**, 319–323.
- 83 K. Hedayatianfard, M. Akhlaghi and H. Sharifiyazdi, *Vet. Res. Forum*, 2014, **5**, 269–275.
- 84 T. Bruna, F. Maldonado-bravo, P. Jara and N. Caro, *Int. J. Mol. Sci. Rev.*, 2021, **7202**, 1–21.
- 85 M. A. Qaeed, A. Hendi, A. S. Obaid, A. A. Thahe, A. M. Osman, A. Ismail, A. Mindil, A. A. Eid, F. Aqlan, N. M. A. Osman, A. A. L. Farga, S. M. Al Maaqar and A. A. Saif, *Sci. Rep.*, 2023, 1–11.
- 86 T. Roshmi, K. R. Soumya, M. Jyothis and E. K. Radhakrishnan, *Gold Bull.*, 2015, **48**, 63–71.
- 87 S. Pansambal, K. Deshmukh, A. Savale, S. Ghotekar, O. Pardeshi, G. Jain, Y. Aher and D. Pore, *J. Nanostruct.*, 2017, **7**, 165–174.
- 88 V. V. T. Padi and M. Cernik, *Int. J. Nanomed.*, 2013, **8**, 889–898.
- 89 J. M. Schuurmans, A. S. Nuri Hayali, B. B. Koenders and B. H. ter Kuile, *J. Microbiol. Methods*, 2009, **79**, 44–47.
- 90 M. Dolati, F. Tafvizi and P. Jafari, *Sci. Rep.*, 2023, 1–19.
- 91 M. Ghasemi, T. Turnbull, S. Sebastian and I. Kempson, *Int. J. Mol. Sci.*, 2021, **22**, 12827.
- 92 S. Sivalingam, A. Kunhilintakath, P. Nagamony and V. Paspulathi Parthasarathy, *Appl. Nanosci.*, 2021, **11**, 679–686.
- 93 W. Wang, M. Liu, B. Yuan, X. Jin, M. Zhu, H. Xu and G. Xie, *Front. Vet. Sci.*, 2021, **8**, 1–14.